The circular polarization of Sagittarius A* at submillimeter wavelengths

Accepted for Publication in the Astrophysical Journal
Preprint typeset using LaTeX style emulateapj v. 12/16/11

THE CIRCULAR POLARIZATION OF SAGITTARIUS A* AT SUBMILLIMETER WAVELENGTHS

D. J. Muñoz[1], D. P. Marrone[2,3,4], J. M. Moran[1], and R. Rao[5]
[1]Harvard-Smithsonian Center for Astrophysics, 60 Garden Street, Cambridge, MA 02138
[2]Kavli Institute for Cosmological Physics, University of Chicago, 5640 South Ellis Avenue, Chicago, IL 60637
[3]Steward Observatory, University of Arizona, 933 North Cherry Avenue, Tucson, AZ 85721
[4]Hubble Fellow
[5]Submillimeter Array, Academia Sinica Institute of Astronomy and Astrophysics, 645 N. Aohoku Place, Hilo, HI 96720
Accepted for Publication in the Astrophysical Journal

ABSTRACT

We report the first detections of circularly polarized emission at submillimeter wavelengths from the compact radio source and supermassive black hole candidate Sgr A* at a level of $1.2 \pm 0.3\%$ at 1.3 mm wavelength (230 GHz) and $1.6 \pm 0.3\%$ at 860 μm (345 GHz) with the same handedness, left circular polarization (LCP), as observed at all lower frequencies (1.4–15 GHz). The observations, taken with the Submillimeter Array in multiple epochs, also show simultaneous linear polarization (LP) at both wavelengths of about 6%. These properties differ sharply from those at wavelengths longer than 1 cm (frequencies below 30 GHz), where weak circular polarization (CP) ($\sim 0.5\%$) dominates over LP, which is not detected at similar fractional limits. We describe an extensive set of tests to ensure the accuracy of our measurements. We find no circular polarization (CP) in any other source, including the bright quasar 1924-292, which traces the same path on the sky as Sgr A* and therefore should be subject to identical systematic errors originating in the instrument frame. Since a relativistic synchrotron plasma is expected to produce little CP, the observed CP is probably generated close to the event horizon by the Faraday conversion process. We use a simple approximation to show that the phase shift associated with Faraday conversion can be nearly independent of frequency, a sufficient condition to make the handedness of CP independent of frequency. Because the size of the $\tau = 1$ surface changes by more than an order of magnitude between 1.4 and 345 GHz, the magnetic field must be coherent over such scales to consistently produce LCP. To improve our understanding of the environment of SgrA* critical future measurements include determining whether the Faraday rotation deviates from a λ^2 dependence in wavelength and whether the circular and linear components of the flux density are correlated.

Subject headings: black hole physics — Galaxy: center — plasmas — polarization — submillimeter — techniques: interferometric

1. INTRODUCTION

The Galactic Center source Sagittarius A* (Sgr A*), the nearest supermassive black hole (SMBH), is extremely underluminous for its mass ($\sim 4 \times 10^6$ $M_\odot$, Ghez et al. 2008; Gillessen et al. 2009), radiating at only $10^{-9}\, L_{\rm Edd}$. Theoretical models have focused their efforts on explaining this faintness by invoking diverse physical mechanisms that result in radiatively inefficient accretion and/or outflow processes (Falcke et al. 1993; Narayan & Yi 1994; Blandford & Begelman 1999; Quataert & Gruzinov 2000; Falcke & Markoff 2000; Yuan et al. 2002). These models adequately reproduce the quiescent spectrum of Sgr A* (Narayan et al. 1998; Markoff et al. 2001; Melia et al. 2001; Yuan et al. 2003), although the spectrum alone does not discriminate between them.

In subsequent years, new observations have provided new types of constraints on the models. Very long baseline interferometry (VLBI) has measured the wavelength-dependent size of Sgr A*, detecting structure on event-horizon scales in the highest frequency/resolution experiments (Shen et al. 2005; Bower et al. 2006; Doeleman et al. 2008; Fish et al. 2011). The size-wavelength relation, and even the observed interferometric visibility of the emission, can be matched by several models (Markoff et al. 2007; Mościbrodzka et al. 2009; Huang et al. 2009b; Broderick et al. 2011). Multiwavelength variability (Marrone et al. 2008; Yusef-Zadeh et al. 2008; Kunneriath et al. 2010), in combination with other observables, which may also reveal information about source structure, can also be replicated in multiple schemes (Dexter et al. 2009; Maitra et al. 2009).

The polarization spectrum and its variability present additional, rich information about source structure. Strong theoretical constraints can be derived by considering the effects of polarized radiative transfer (PRT) in the models. Perhaps the simplest and most common consequence of PRT through a plasma is Faraday rotation of linear polarization (LP). In recent years, multifrequency millimeter and submillimeter polarimetry has allowed measurements of Faraday rotation in Sgr A*(Marrone et al. 2006a, 2007). These data have provided bounds on the accretion rate in the inner regions of the flow (Macquart et al. 2006; Marrone et al. 2007).

A synchrotron-emitting plasma can be expected to produce significant LP fractions at frequencies near the spectral peak. At the same time, these relativistic plas-

dmunoz@cfa.harvard.edu
January 18, 2014

TABLE 1
Radio-to-Submillimeter Linear and Circular Polarization of Sgr A*

Frequency (GHz)	Fractional LP (%)[a]	Fractional Stokes V (%)[b]	Reference
1.4	···	-0.21 ± 0.10 (13)	Bower et al. (2002)
4.8	···	-0.33 ± 0.07 (13)	”
8.4	···	-0.32 ± 0.08 (13)	”
15	···	-0.62 ± 0.26 (12)	”
4.8	···	-0.37 ± 0.04	Sault & Macquart (1999)
4.8	< 0.08	···	Bower et al. (1999a)
8.4	< 0.17	···	”
4.8	···	-0.36 ± 0.05 (3)	Bower et al. (1999b)
8.4	···	-0.26 ± 0.06 (3)	”
22	< 0.2	···	Bower et al. (1999c)
43	< 0.4	···	”
86	< 1.0	···	”
82.8	2.1 ± 0.4	···	Macquart et al. (2006)
86.3	0.8 ± 0.5	···	”
100	···	< 2.0	Tsuboi et al. (2003)
112	< 3.6	< 3.6	Bower et al. (2001)
216	9.1 ± 2.2	···	Bower et al. (2005)
230	10.0 ± 2.5	···	”
230	7.2 ± 0.6	$\lesssim 2$	Bower et al. (2003)
230	5.9 ± 1.6	···	Marrone et al. (2007)
340	6.4 ± 2.0	$\lesssim 1$	Marrone et al. (2006a)
150	12^{+9}_{-4}	···	Aitken et al. (2000)
225	11^{+3}_{-2}	···	”
350	13^{+10}_{-4}	···	”
400	22^{+25}_{-9}	···	”

[a] Uncertainties can correspond to both systematic errors and time-variability dispersion. For example, data corresponding to the multi-epoch observations of Marrone et al. (2006a, 2007) are presented with errors corresponding to the standard deviation of the sample.
[b] The errors shown are the standard deviation (rms) of the sample, not the standard deviation of the mean. The number of samples is listed in parentheses. For the Bower et al. (2002) data, we show the results for the 1999 VLA measurements only because of the advanced calibration technique used. However, they are consistent with the archival VLA and the ATCA data also reported by Bower et al. (2002). Upper limits are shown at the 2-σ level.

mas are expected to produce very small amounts of circular polarization (CP) by intrinsic emission of Stokes V (Landau & Lifshitz 1975) or through various radiative transfer effects (e.g., Jones & Odell 1977; Melrose 1997; Ruszkowski & Begelman 2002; Shcherbakov 2008). As the polarization arises very near to the black hole, a full picture of the emergent polarization state can diagnose both the inner regions and the intervening propagation medium.

A compilation of published polarization measurements is given in Table 1 and shown in Figure 1. No LP has been observed at 8 GHz or below at limits of 0.2% or less (Bower et al. 1999a). The LP of Sgr A* was first detected by Aitken et al. (2000) above 100 GHz. These measurements were obtained with large beams (7″–22″) and required background subtraction, leaving some uncertainty about residual polarization contamination from the surrounding dust emission. Subsequent interferometer observations at millimeter and submillimeter wavelengths have shown polarization at the level of 1–10%, which varies in position angle (Bower et al. 2005) and fraction (Marrone et al. 2006a) with timescales comparable to those of previously observed total intensity variations (Marrone et al. 2006b). The variability may be intrinsic to the source or due to propagation effects, but the short timescales involved suggest that processes very close to the SMBH are responsible. The LP was measured simultaneously at multiple frequencies for the first time by Marrone et al. (2007). The inferred rotation measure (RM) indicates that Sgr A* is extremely underfed, with an accretion rate of $\sim 10^{-8}\, M_\odot\ \mathrm{yr}^{-1}$.

CP from Sgr A* was first detected by Bower et al. (1999b). Later, Bower et al. (2002) reported spectral measurements between 1.4 and 15 GHz as well as time variability of CP (see lower panel in Figure 1). They concluded that the time-averaged CP spectrum is approximately $\nu^{0.5\pm0.2}$, with persistent variability that increases with frequency. They also noted that the sense of CP for all available measurements (about 100 measurements from 1981 to 1999, made with both the VLA and ATCA at 1.4, 4.8, and 15 GHz) was exclusively LCP, indicative of a long-term stability in magnetic field configuration. At these frequencies, LP is not detected down to instrumental limits of 0.1% while CP is persistently detected at levels of a fraction of a percent with a degree of variability of the same order of magnitude. This is substantially different from what is seen in high-luminosity active galactic nuclei (AGN), where LP always dominates CP. Above roughly 100 GHz, LP becomes dominant in Sgr A*, with CP undetectable at ∼1% sensitivity. In four epochs of 230 GHz observations, Bower et al. (2003) found a 2-σ CP signal (3%) on one day, with an average measurement of $1\% \pm 1\%$. No CP was observed at a level of 0.5% in the 100 GHz data reported by Tsuboi et al. (2003). Marrone et al. (2006a) measured V at 345 GHz and obtained $-0.5 \pm 0.3\%$. However, because of systematic calibration uncertainties, they reported this result as an upper limit of 1.5%.

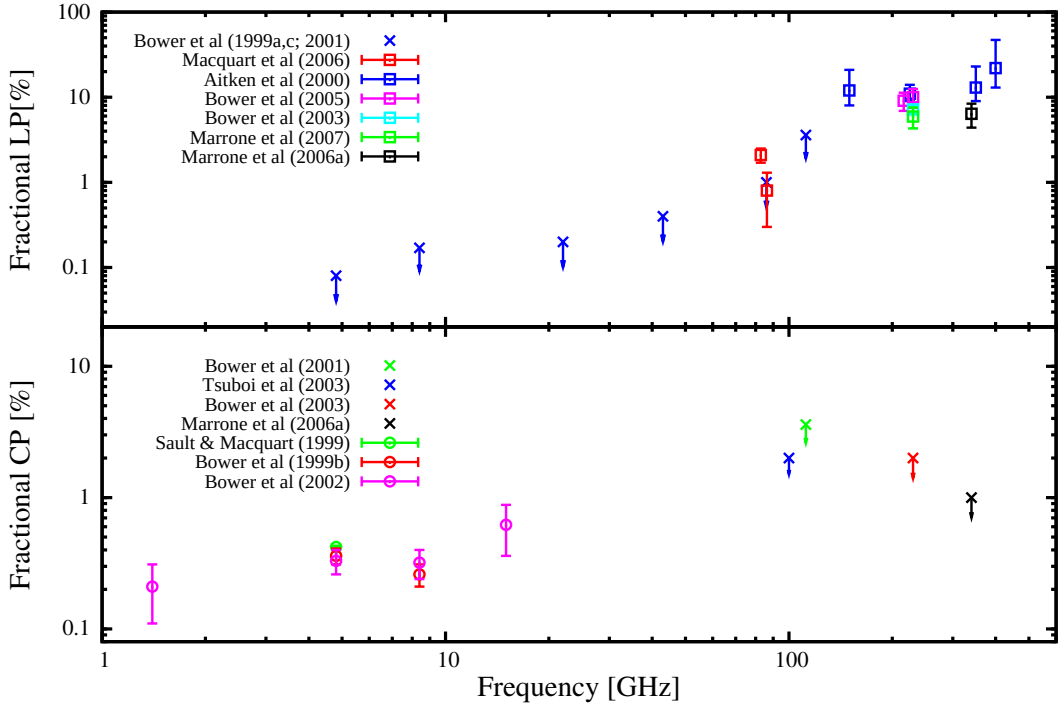

FIG. 1.— Published measurements of the fractional linear and circular polarization toward Sgr A* as a function of frequency.

CP is also observed in a variety of radio sources, including pulsars and AGN. Examples are 3C273 and 3C279 (Homan & Wardle 1999). Some models seeking to explain the millimeter and submillimeter LP have also predicted CP at these high frequencies due to the conversion of LP to CP in a turbulent jet (e.g., Beckert & Falcke 2002). In these models, in addition to the stochasticity of the magnetic field—which appears to play a crucial role in building up CP by propagation effects—the helical geometry of jets might be important in high levels of LP, above 100 GHz.

Coupled mechanisms to produce both LP and CP in relativistic outflows have been studied in detail by many authors (e.g., Ruszkowski & Begelman 2002; Beckert & Falcke 2002; Beckert 2003; Huang et al. 2008; Homan et al. 2009; Shcherbakov et al. 2010). If CP is produced predominantly by propagation effects, multifrequency measurements of RM and CP can provide important clues about the magnetic field structure of the plasma surrounding the SMBH. Similarly, simultaneous measurements of LP and CP variability can determine whether the intraday variability in Sgr A* is due to intrinsic variations in the central engine or to variations in the outer layers of the accretion flow. In this way, it should be possible to conclusively infer the presence or absence of a "Faraday screen" in front of Sgr A* (Macquart et al. 2006; Marrone et al. 2007).

In Section 2 we describe several epochs of polarimetric observations of Sgr A*, Section 3 reports the observed polarization, and Section 4 explores the tests of systematic errors in the observations that might give rise to false CP. Section 5 reviews PRT and the astrophysical mechanisms for generating CP, and their applicability to Sgr A*.

TABLE 2
OBSERVATION EPOCHS

Date	Main Target	Freq.[a] [GHz]	SMA Config.[b]	$\tau_{225\,\mathrm{GHz}}$
2005 June 6	Sgr A*	343.0	CN	0.055
2006 July 17	Sgr A*	226.9	VEX	0.05-0.08
2007 March 31	Sgr A*	226.9	CN	0.055
2008 May 30	1924-292	226.9	CN	0.08

[a] Frequency of the local oscillator. Upper and lower sidebands are centered 5 GHz above and below this frequency, respectively.
[b] Array configurations include "Compact North" (CN) and "Very Extended" (VEX).

2. OBSERVATIONS

The data presented in this work consist of three polarimetry tracks (Table 2) taken with the Submillimeter Array (SMA).[1] The general characteristics of the SMA are described by Blundell (2004) and Ho et al. (2004), and its polarimeter is described by Marrone (2006) and Marrone & Rao (2008). The most significant detection of CP at 230 GHz was made from the observations of March 31, 2007. Archival data from two other observations—one at 230 GHz and another at 345 GHz—were analyzed to confirm and extend the initial result. A typi-

[1] The Submillimeter Array is a joint project between the Smithsonian Astrophysical Observatory and the Academia Sinica Institute of Astronomy and Astrophysics and is funded by the Smithsonian Institution and the Academia Sinica.

TABLE 3
Double-Sideband Flux and (Fractional) Polarization for Sgr A*

Date	Freq. [GHz]	I^a [Jy]	Q/I	U/I	V/I
2005 June 6	343.0	3.17 ± 0.02	0.027 ± 0.003	-0.049 ± 0.003	-0.016 ± 0.003
2006 July 17	226.9	3.88 ± 0.02	0.020 ± 0.003	-0.053 ± 0.003	-0.011 ± 0.003
2007 March 31	226.9	3.52 ± 0.01	-0.061 ± 0.001	-0.032 ± 0.001	-0.012 ± 0.001
2008 May 30[b]	226.9	3.87 ± 0.02	0.044 ± 0.002	-0.032 ± 0.002	-0.011 ± 0.004

[a] Statistical error only. Absolute calibration precision is typically 10-20%.
[b] Sgr A* was observed for one hour prior to the 1924-292 test observation.

cal Sgr A* polarimetry track consisted of ~ 12 hours of observations, of which ~ 6 corresponded to continuous monitoring of Sgr A*. The quasar 1733-130 was used as the gain calibrator of Sgr A*, while quasars 3C273 and 3C279 were used to calibrate for instrumental polarization (leakage). In addition, quasars such as 1337-129 and 3C286 were commonly included in the tracks, as well as a solar system object (e.g., Titan) for flux density calibration.

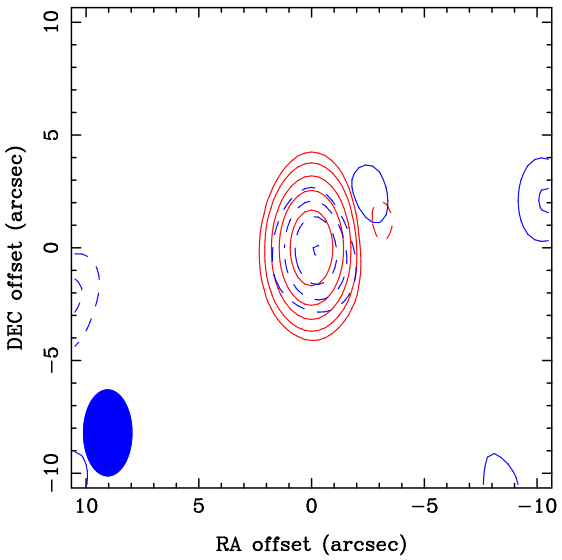

Fig. 2.— Total and CP emission of Sgr A* (March 31, 2007): red contours correspond to Stokes I flux density while blue contours correspond to Stokes V flux density. Solid and dashed contours indicate positive and negative flux density, respectively. Stokes I contour spacings are $-6, 6, 12, 25, 50, 100 \times \sigma_I$, where $\sigma_I = 19.8$ mJy/beam is the rms noise in the I map. The contour levels for the Stokes V map are $-11, -7, -4, -2, 2, 4 \times \sigma_V$, where $\sigma_V = 2.9$ mJy/beam is the rms noise in the V map.

To test the accuracy of our CP measurement, we made a special observation of the quasar 1924-292 at 230 GHz on May 30, 2008, along with another short-track measurement of Sgr A*. 1924-292 has nearly the same declination as Sgr A*, so both have the same AZ–EL track and, hence, position angle dependence with time. This track also contained a one-hour segment on Sgr A*. The gain calibrator for 1924-292 was 1911-201, and the polarization calibrators were 3C273 and 3C279. Every effort was made to keep the observational circumstances identical to those of previous tracks (e.g., same polarization sampling cycle).

The SMA polarimeter allows precise gain calibration for the RR and LL visibilities. A single quarter-wave plate is located in the beam of each telescope and rotates to produce either right CP or LCP. The polarization of each antenna is modulated according to orthogonal Walsh functions of period 16 to efficiently sample all four polarization combinations on each baseline. Quasi-simultaneous polarization data are generated in post-processing by averaging over the switching cycle. The use of the same waveplate and feed for both R and L polarization states eliminates some of the uncertainties inherent in the use of dual-feed receivers, particularly differential phase variations between the polarization states. Measurement of LP (Stokes Q and U) relies on precise determination of the leakage of each polarization state by the crosshanded polarization, which was performed using linearly polarized bright point sources (quasars 3C279 or 3C273) observed over a large range of parallactic angle. To first order, these leakages do not affect the measurement of Stokes V (e.g., Marrone 2006; Thompson et al. 2001, and Section 4.1), leaving the relative calibration of the RR and LL visibilities as the primary calibration challenge for measurement of Stokes V.

3. RESULTS

The polarization measurements (Stokes I, Q, U, and V) of Sgr A* for four different epochs included in our analysis are shown in Table 3. The flux densities for each Stokes parameter I, Q, U, and V were obtained by fitting a point-source model to the visibilities, fixing the position to the phase center of the observations, the location of Sgr A*. The polarization Stokes parameters are listed as a fraction of the total flux density. For four different epochs—including different frequencies, different uv-space sampling, and a time span of three years—Sgr A* is shown consistently to be circularly polarized at the $\gtrsim 1\%$ level. The sense of CP (negative V) persists throughout.

Figure 2 shows the contour maps for both Stokes I and V for the whole track of March 31, 2007. In this case, the measured CP flux density is -41 ± 3 mJy (in the standard IAU sign convention, where a negative sign indicates LCP), corresponding to $\sim -1.2\%$ of the total flux density. The background rms noise of the image is 3.1 mJy beam^{-1}, consistent with the statistical error of ± 3 mJy obtained from the visibility fit. Figure 3 shows the compilation of published CP observations from the lower panel of Figure 1 along with our new measurements. Although there are many unobserved frequencies, the polarization appears to increase monotonically with frequency while retaining the same handedness throughout. The CP spectrum scales approximately as $\nu^{0.35 \pm 0.03}$ across the range of frequencies with detections. Subdi-

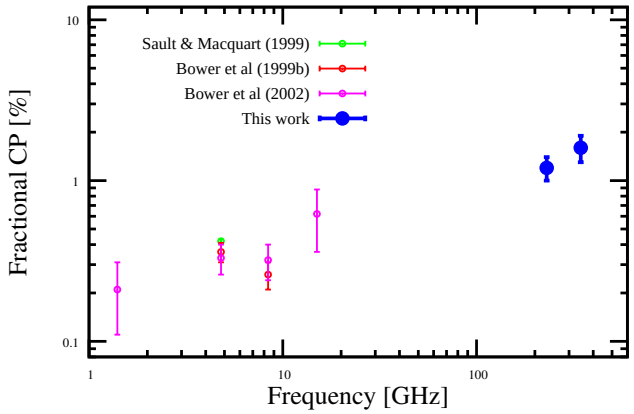

FIG. 3.— Fractional CP in Sgr A* (LCP in all cases) from radio to submillimeter frequencies (lower panel in Figure 1), including the new SMA data (see Table 3). The percentage of CP increases with frequency as $\sim \nu^{0.35\pm0.03}$.

viding the track into four segments, (see Figure 4 and Table 4), we see no statistically significant variability in the CP, with the largest change corresponding to a 2-σ difference. We limit fractional variation in the CP, i.e., $\Delta V/V$, at the 2-σ level of significance to 40%, which is comparable to the fractional changes in CP at 1−15 GHz measured by Bower et al. (2002). There is a tantalizing correlation at the 2-σ level of significance between the circularly and linearly polarized flux densities. However, with only four data points, so significant conclusion can be drawn.

Figure 2 shows a slight offset between the peak positions of V and I. This offset, 0.18 arcseconds, is consistent with what is expected for an SNR of ∼14. The offset is observed in all of the Sgr A* polarimetric tracks at all frequencies, and the orientation and angular amplitude of the offset vary with time within a single track. This shift between the peaks of the Stokes V and Stokes I images suggests imperfection in our CP calibration procedure. The offset is barely noticeable for maps derived from complete tracks (e.g., Figure 2), but it becomes significantly larger when the track is split into consecutive time intervals (see Figure 4 and Table 4). The fact that the offset grows when reducing the SNR suggests that the wandering of the Stokes V map around the Stokes I may be in part due to a thermal noise effect. However, extensive tests (Section 4) suggest that the offset is not dominated by noise.

Table 5 shows the polarization flux densities for all the test quasars observed on March 31, 2007. All point-source flux densities are obtained from the visibility fitting process. Quasars 3C273, 3C279, 3C286, 1337-129, and 1733-130 show CP fractions consistent with zero in both sidebands. The deviations from zero are of the same sign for all objects, which suggests a systematic error that would fractionally apply to Sgr A* as well. However, the 0.1% weighted-average magnitude (right CP) of this systematic error is negligibly small, an order of magnitude smaller than the observed CP in Sgr A*.

The circular polarization of quasar 1924-292 (last line of Table 5) was also measured in a separate track on May 30, 2008. The V flux determined by a point-source fit to the visibilities, constrained to lie at the pointing center, is consistent with zero, as for the other sources. However, within a region comparable in size to the synthesized beam, the Stokes V signal varies between $+5\sigma$ and -4σ, as shown in Figure 5. This antisymmetric pattern and other calibration effects are discussed in detail in Section 4.3.

4. ERROR INSPECTION AND POLARIZATION TESTS

The consistency of the measurements in Table 3 over a period of three years and at multiple frequencies suggests a robust detection of CP. The most sensitive of the detections has a significance of greater than 10σ. Because our work presents the first measurements of CP with the SMA, we feel it is important to describe our calibration methods and system checks in detail.

4.1. *Polarization Calibration*

In an ideal interferometer with circularly polarized feeds, CP in a target source appears as a difference between the parallel-hand visibilities. Complications may arise due to imperfection in the interferometer response and calibration. The four polarized visibilities in a circularly polarized interferometer can be written (Thompson et al. 2001):

$$\begin{aligned}
\mathcal{V}_{RR} &= g_{Ra}g^*_{Rb}\left[(\mathcal{V}_I+\mathcal{V}_V)+d_{Ra}d^*_{Rb}\,(\mathcal{V}_I-\mathcal{V}_V)\right.\\
&\left.+\,d_{Ra}\,(\mathcal{V}_Q-i\mathcal{V}_U)\,e^{2i\phi}+d^*_{Rb}\,(\mathcal{V}_Q+i\mathcal{V}_U)\,e^{-2i\phi}\right]\\
\mathcal{V}_{RL} &= g_{Ra}g^*_{Lb}\left[(\mathcal{V}_Q+i\mathcal{V}_U)\,e^{-2i\phi}+d_{Ra}\,(\mathcal{V}_I-\mathcal{V}_V)\right.\\
&\left.-d^*_{Lb}\,(\mathcal{V}_I+\mathcal{V}_V)-d_{Ra}d^*_{Lb}\,(\mathcal{V}_Q-i\mathcal{V}_U)\,e^{2i\phi}\right]\\
\mathcal{V}_{LR} &= g_{La}g^*_{Rb}\left[(\mathcal{V}_Q-i\mathcal{V}_U)\,e^{2i\phi}-d_{La}\,(\mathcal{V}_I+\mathcal{V}_V)\right.\\
&\left.+d^*_{Rb}\,(\mathcal{V}_I-\mathcal{V}_V)-d_{La}d^*_{Rb}\,(\mathcal{V}_Q+i\mathcal{V}_U)\,e^{-2i\phi}\right]\\
\mathcal{V}_{LL} &= g_{La}g^*_{Lb}\left[(\mathcal{V}_I-\mathcal{V}_V)+d_{La}d^*_{Lb}\,(\mathcal{V}_I+\mathcal{V}_V)\right.\\
&\left.-d_{La}\,(\mathcal{V}_Q+i\mathcal{V}_U)\,e^{-2i\phi}-d^*_{Lb}\,(\mathcal{V}_Q-i\mathcal{V}_U)\,e^{2i\phi}\right] \quad ,
\end{aligned}$$

where g_{Ra} and g_{La} (d_{Ra} and d_{La}) are the right and left circular feed gains (polarization leakage terms) of antenna a, and ϕ is the parallactic angle of the feed. Solving the linear system of equations above for the Stokes I and the Stokes V visibilities, respectively, gives

$$\begin{aligned}
\mathcal{V}_I = &\frac{\mathcal{V}_{RR}}{2g_{Ra}g^*_{Rb}}\frac{(1+d_{La}d^*_{Lb})}{(1+d_{Ra}d_{La})(1+d^*_{Rb}d^*_{Lb})}\\
&+\frac{\mathcal{V}_{LL}}{2g_{La}g^*_{Lb}}\frac{(1+d_{Ra}d^*_{Rb})}{(1+d_{Ra}d_{La})(1+d^*_{Rb}d^*_{Lb})}\\
&+\frac{\mathcal{V}_{RL}}{2g_{Ra}g^*_{Lb}}\frac{(d_{La}-d^*_{Rb})}{(1+d_{Ra}d_{La})(1+d^*_{Rb}d^*_{Lb})}\\
&+\frac{\mathcal{V}_{LR}}{2g_{La}g^*_{Rb}}\frac{(d^*_{Lb}-d_{Ra})}{(1+d_{Ra}d_{La})(1+d^*_{Rb}d^*_{Lb})}
\end{aligned} \tag{1}$$

and

$$\begin{aligned}
\mathcal{V}_V = &\frac{\mathcal{V}_{RR}}{2g_{Ra}g^*_{Rb}}\frac{(1-d_{La}d^*_{Lb})}{(1+d_{Ra}d_{La})(1+d^*_{Rb}d^*_{Lb})}\\
&-\frac{\mathcal{V}_{LL}}{2g_{La}g^*_{Lb}}\frac{(1-d_{Ra}d^*_{Rb})}{(1+d_{Ra}d_{La})(1+d^*_{Rb}d^*_{Lb})}\\
&-\frac{\mathcal{V}_{RL}}{2g_{Ra}g^*_{Lb}}\frac{(d_{La}+d^*_{Rb})}{(1+d_{Ra}d_{La})(1+d^*_{Rb}d^*_{Lb})}\\
&-\frac{\mathcal{V}_{LR}}{2g^*_{Rb}g_{La}}\frac{(d_{Ra}+d^*_{Lb})}{(1+d_{Ra}d_{La})(1+d^*_{Rb}d^*_{Lb})} \quad .
\end{aligned} \tag{2}$$

TABLE 4
Circular Polarization in Subsections of March 31, 2008 Track

UT hour range	V/I	$\Delta\theta_V$ (arcsec)	SNR_V
12.4 -14.2	$(-1.3 \pm 0.2) \times 10^{-2}$	1.52 ± 0.27	6.5
14.2 -15.7	$(-1.1 \pm 0.1) \times 10^{-2}$	0.78 ± 0.21	7.8
15.7 -17.2	$(-1.6 \pm 0.1) \times 10^{-2}$	0.77 ± 0.10	10.5
17.2 -18.9	$(-1.6 \pm 0.2) \times 10^{-2}$	0.31 ± 0.18	9.1

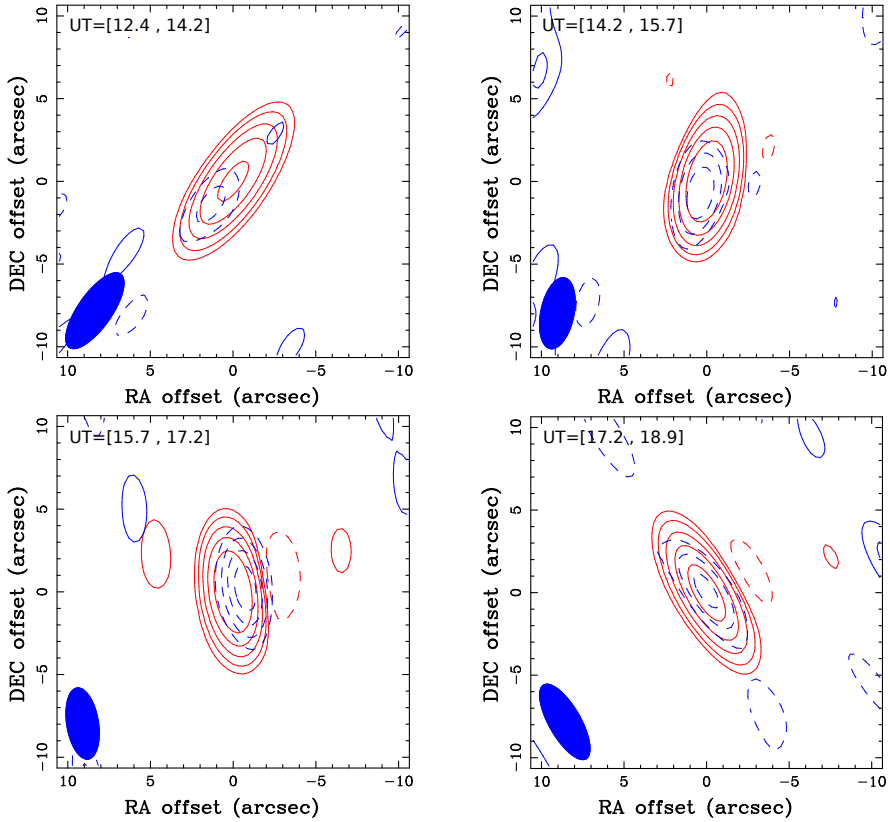

Fig. 4.— Contour images of Sgr A* made from four segments of the track on March 31, 2007. Red: Stokes I in Jy/beam. Blue: Stokes V in Jy/beam. The color coding and contour levels are the same as in Figure 2. Each of the four panels corresponds to one of the four time intervals the track was divided into: UT=13.4, 14.9, 16.4, and 17.9 hours.

To first order in the leakages d, and ignoring terms proportional to $\mathcal{V}_{LR}\,d$ and $\mathcal{V}_{RL}\,d$ (small LP as well as small leakages), we have

$$\mathcal{V}_I \simeq \frac{1}{2}\left\{\,\mathcal{V}_{RR}/(g_{Ra}g^*_{Rb}) + \mathcal{V}_{LL}/(g_{La}g^*_{Lb})\right\} \qquad (3)$$

and

$$\mathcal{V}_V \simeq \frac{1}{2}\left\{\,\mathcal{V}_{RR}/(g_{Ra}g^*_{Rb}) - \mathcal{V}_{LL}/(g_{La}g^*_{Lb})\right\} \quad , \qquad (4)$$

and thus Stokes I and V are independent of the leakages to first order.

The MIRIAD reduction package (Sault et al. 1995) uses these first-order equations when solving for the polarized leakages, ignoring second-order terms in the leakages d and LP fraction. These terms contribute a systematic error in Stokes V of the form Id^2 and md, for LP fraction m. For the track of March 31, 2007, all leakage terms are of order $\sim 10^{-2}$ (both real and imaginary parts), introducing a fractional contribution from Stokes I of $\sim 10^{-4}$. Likewise, the terms of order md are of order 10^{-3} and are unable to explain the observed CP fraction of 10^{-2}. Another uncertainty arises from the complex terms dependent on the parallactic angle in the form of a phase term in the full gain equations. A systematic phase effect could, in principle, explain offsets in the image plane; however, the low flux density contribution from these offset components ($\sim md$) makes this possibility difficult to reconcile with the evident displacement of the entire point-source flux density in Figure 4.

4.2. *Gain Calibration*

Errors in the relative calibration of the L and R gains of the antennas affect the precise cancellation of terms in eq. 4 and are the most natural way to generate false CP. The time variation of the antenna gains is monitored using 1733-130, which, at a flux density of ∼1 Jy, is much weaker than Sgr A*. In order to maximize the

TABLE 5
CIRCULAR POLARIZATION[a] FOR TEST QUASARS ON MARCH 31, 2007

	LSB		USB	
Source	I [Jy]	V/I	I [Jy]	V/I
3C273[b]	15.40 ± 0.03	$(1.2 \pm 1.2) \times 10^{-3}$	15.05 ± 0.02	$(1.1 \pm 1.3) \times 10^{-3}$
3C279	12.92 ± 0.02	$(1.5 \pm 1.4) \times 10^{-3}$	12.88 ± 0.02	$(1.3 \pm 1.4) \times 10^{-3}$
3C286	0.49 ± 0.01	$(7.9 \pm 15.2) \times 10^{-3}$	0.46 ± 0.01	$(14.8 \pm 17.9) \times 10^{-3}$
1337-129	6.92 ± 0.03	$(2.1 \pm 3.0) \times 10^{-3}$	6.89 ± 0.03	$(2.5 \pm 3.4) \times 10^{-3}$
1733-130[c]	1.48 ± 0.04	$(0.8 \pm 0.4) \times 10^{-3}$	1.46 ± 0.04	$(1.0 \pm 0.5) \times 10^{-3}$
1924-292[d]	7.00 ± 0.01	$(-0.2 \pm 1.1) \times 10^{-3}$	6.95 ± 0.01	$(-0.1 \pm 1.2) \times 10^{-3}$

[a] Stokes V fluxes were calculated by fitting the visibility data to visibilities corresponding to a point source located at the interferometric (phase) center of the map.
[b] 3C273 was calibrated in polarization and gain with 3C279. In contrast, quasars 3C279, 3C286, and 1337-129 were calibrated using 3C273 as a gain and a polarization calibrator.
[c] Quasar 1773-130 is the gain calibrator for Sgr A*. The average gain curve was derived using both LL and RR visibilities, then applied to the 1733-130 data before measuring the CP.
[d] Shown here for comparison, quasar 1924-292 was observed on the night of May 30, 2008.

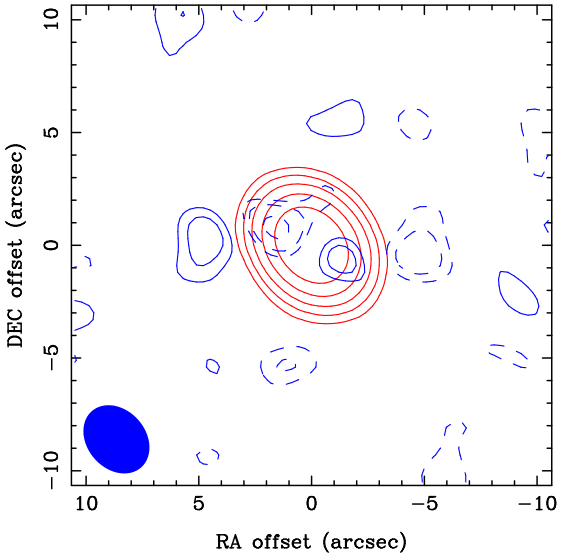

FIG. 5.— Total and CP emission of 1924-292. Color coding is identical to Figure 2. Stokes I contour spacings are $12, 25, 50, 100, 200 \times \sigma_I$, where $\sigma_I = 14.7$ mJy/beam is the rms noise in the I map. The contour levels for the Stokes V map are $-5, -3, -2, 2, 3 \times \sigma_V$ where $\sigma_V = 5.85$ mJy/beam is the rms noise in the V map. Within the angular extent of the Stokes I point source, two distinct Stokes V are identifiable. The negative peak corresponds to approximately −30 mJy/beam (i.e., −0.4% of the Stokes I peak), and the positive one corresponds to approximately +18 mJy/beam (i.e., 0.25% of the Stokes I peak).

signal-to-noise of the gain measurements, we choose to average the amplitude of the LL and RR visibilities together and determine a single gain curve per antenna rather than separately measuring g_L and g_R. If there is an imbalance in the response of the two "feeds," which are really the same receiver looking through the same quarter-wave plate, this will introduce false CP.

The first test of our calibration method is to examine the calibrated 1733-130 data for CP. In Table 5 we report the polarization measured in 1733-130 after applying the same gains that are used with the Sgr A* data. Although we make no attempt to correct the difference in the L and R gains in our calibration procedure, we end up with little polarization in this source (<0.1%), with a fractional V sensitivity of $\sim 5 \times 10^{-4}$. This suggests a systematic polarization limit of 10^{-3} for this calibration method. Performing the calibration with separate gains for L and R yields nearly identical results for the polarization fraction of Sgr A* but with slightly higher noise.

A second test of this calibration method is to examine the V/I measured for other quasars in the track. We expect no significant CP in quasars at these wavelengths. Figure 6 and Table 5 show that no CP is found in the quasars observed in the March 31, 2007, track. Fractional polarization limits are comparable to those obtained on 1733-130, except for 3C286, which is significantly fainter than the others and thus has a higher level of noise in V/I.

4.3. *Circular Polarization of 1924-292*

To guard against poorly understood instrumental effects that preferentially affect, for example, sources at low elevation or those with poor parallactic angle coverage, we undertook a supplementary test using the quasar 1924-292. The declination of this source is within half a degree of that of Sgr A*, ensuring that it follows the same path on the sky. The observation scheme was designed to precisely mimic that of the primary track on Sgr A*, with similar hour angle coverage and temporal sampling, identical polarization modulation, and a gain calibrator (1922-201) at a similar distance from the target (9° north compared to 16° for 1733-130 and Sgr A*). Because 1924-292 was brighter at the time of these observations, 7 Jy, than Sgr A* was during the other observations (3–4 Jy), and because of the long integration time in the track, this test also provides a more sensitive limit on instrumental CP than the that provided by observations of quasars on March 31, 2007.

The results of this test are shown in Figure 5 and the last line of Table 5. Fitting the visibilities to a point source, as was done for other quasars and Sgr A*, we find $V/I = 1 - 2 \times 10^{-4}$, with an uncertainty of 10^{-3}. This is a factor of more than 10 lower than the CP fraction observed in Sgr A*, including that measured in the same track in a short observation (last line, Table 3). That the polarization of 1924-292 was not found at the same time that the previously observed CP level in Sgr A* was reconfirmed enhances our confidence in our result.

Figure 5 does show significant CP in an antisymmet-

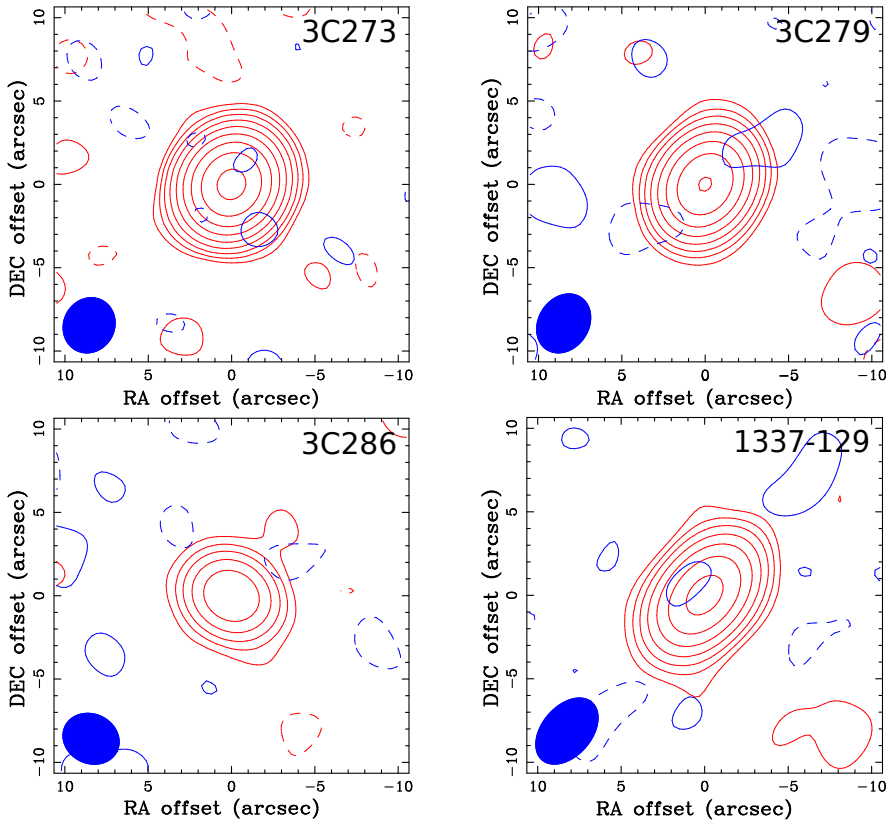

FIG. 6.— Quasars 3C273, 3C279, 3C286, and 1337-129 observed during the track of March 31, 2007, after gain calibration using 3C273 as calibrator. Each image shows contour plots in Stokes I and V in the same way as Figure 2. For each panel, the contours in Stokes V are –2 and 2 times the rms noise of the image, and all four of them have maxima and minima between $-3\sigma_V$ and $+3\sigma_V$. The intensity contours in Stokes I are $(-2, 2, 5, 10, 20, 40, 80, 160, 320, 640) \times \sigma_I$ for 3C273 and 3C279. For 3C286 and 1337-129, the contour levels are $(-2, 2, 5, 10, 20, 40)$ and $(-2, 2, 5, 10, 20, 40, 80, 160) \times \sigma_I$, respectively.

ric pattern around the pointing center, with a peak V/I values of $+2.5$ and -4.2×10^{-3}. The negative peak is approximately five times the image rms. The antisymmetric pattern is clearly distinguishable from the offset CP detections in Sgr A*, which do not show peaks of opposite sign one resolution element away from the main peak. We conclude that this is a signature of an unrelated calibration problem. This calibration could mask a peak in the V map that is offset from the pointing center as seen in Sgr A* in Figure 4, with the allowed amplitude being approximately the difference in the positive and negative peaks, or -1.7×10^{-3}. We take this as a limit on our uncorrected instrumental polarization, $V/I < 2 \times 10^{-3}$.

The LP of 1924-292 was measured to be 10.8% during this track, larger than was observed in the Sgr A* tracks in this work. The increased LP makes this source slightly more susceptible to errors from ignored second-order terms from feed imperfections (Section 4.1). Nevertheless, no significant CP is detected.

4.4. *Other Possible Sources of Error*

In the tests discussed thus far, we failed to find CP in any source other than Sgr A*, placing tight limits on the possible instrumental contribution to the observed signal. The previous section describes the most stringent test, which mimics everything about the Sgr A* observation and nevertheless finds insignificant CP in a bright test source.

A possible distinction between the test sources and Sgr A* is the presence of extended emission in our Galactic Center. The test sources are nearly pointlike (with some low-level emission from jet knots in the case of 3C279), while Sgr A* is embedded in dust and free-free emission. To avoid contamination from larger-scale emission, we exclude baselines shorter than 20 kλ from our visibility fits and find that the same exclusion in other sources does not change our results. We are not aware of a mechanism by which the extended emission could introduce false CP, but we have also attempted to verify that no such effect is present. We examined a data set from July 17, 2006, which measures uv spacings of 27–390 kλ instead of the 5–50 kλ that is typical of the other tracks. This track should be more immune to the larger scale emission, which is highly suppressed by the shorter fringe spacing. We see no significant difference in Table 3 between this track and the others.

5. ASTROPHYSICAL SOURCES OF CIRCULAR POLARIZATION

The polarization state of radiation emerging from an astrophysical source is governed by radiative transfer equations that, in their most complete form, incorporate emission and absorption in each Stokes parameter. This polarized radiative transfer equation must also include mixing between Stokes parameters that takes place in

birefringent media, such as a synchrotron plasma. The magnetic field that is fundamental to the synchrotron emission and self-absorption is also a source of birefringence. Variations in the magnetic field along the line of sight, and the change in the coupling between Stokes parameters with plasma temperature, complicate the picture further. A fully consistent treatment requires addressing all these effects simultaneously.

5.1. *Polarized Transfer in a Homogeneous Magnetic Field*

Sgr A*, a stratified, self-absorbed synchrotron source (see de Bruyn 1976, for the basics of these models) with frequency- and time-variable polarization, clearly requires a sophisticated radiative transfer model. The Faraday rotation inferred from submillimeter observations (Marrone et al. 2007) has been assumed to be separate from the submillimeter emission regions, although it may instead occur deep inside the source (sometimes referred to as *internal Faraday rotation*, e.g., Wardle & Homan 2003). The production of CP may similarly be a signature of conversion processes within the emission region. The complete PRT equation is (e.g., Sazonov 1969)

$$\frac{d}{dl}\begin{pmatrix} I \\ Q \\ U \\ V \end{pmatrix} = \begin{pmatrix} \eta_I \\ \eta_Q \\ 0 \\ \eta_V \end{pmatrix} + \begin{pmatrix} -\kappa_I & -\kappa_Q & 0 & -\kappa_V \\ -\kappa_Q & -\kappa_I & -\kappa_V^* & 0 \\ 0 & +\kappa_V^* & -\kappa_I & -\kappa_Q^* \\ -\kappa_V & 0 & +\kappa_Q^* & -\kappa_I \end{pmatrix} \begin{pmatrix} I \\ Q \\ U \\ V \end{pmatrix} \quad (5)$$

where the cartesian axes in the plane of the sky ($\hat{\mathbf{e}}_1$ and $\hat{\mathbf{e}}_2$)—which determine the precise definition of Stokes Q and U—are oriented such that $\hat{\mathbf{e}}_1$ is aligned with the local direction of the magnetic field. The absence of transport coefficients related to Stokes U in eq. 5 is a direct consequence of this convenient choice of coordinates, and thus it is a valid expression only locally.

Eq. 5 is the vectorial generalization of the standard radiative transfer equation $dI_\nu/dl = j_\nu - \alpha_\nu I_\nu$. The η_A (with $A = I, Q, U, V$) are the emission coefficients for each Stokes parameter. The absorption coefficients κ_A (one for each Stokes parameter) are related to the η_A through detailed balance. The antisymmetric portion of the matrix comprises the Faraday transport coefficients κ_A^*. They couple Q, U, and V, permitting exchanges of LP and CP along the path of radiation. This rotation in three-dimensional polarization space (Q, U, V) has been referred to as the *generalized Faraday rotation* effect (Melrose 1997). The general Faraday effect reduces to pure Faraday rotation (i.e., rotation in the Q–U plane) in the nonrelativistic limit and to pure Faraday conversion (i.e., rotation in a plane perpendicular to the Q–U plane) in the ultrarelativistic limit but, in general, is a combination of both.

The intrinsic emission term in eq. 5 (η_V) demonstrates the first potential source of CP. The intrinsic emission in Stokes V is weak: η_V is of order $1/\gamma$ smaller than the other components and is generally ignored in synchrotron emitting plasma. On the other hand, predominantly CP emission can be expected in a cold cyclotron emitting plasma (e.g., Landau & Lifshitz 1975), in which the relativistic approximations intrinsic to synchrotron spectra (e.g., beaming, see Rybicki & Lightman 1979) are not valid (see also Mahadevan et al. 1996). The submillimeter emission from Sgr A* is expected to arise at very small radius where the plasma is hot, and therefore emission from cold electrons is not expected to be relevant.

The birefringence of the plasma may also transform LP to CP, as noted above, but this "Faraday conversion" is weak in a cold plasma. In this limit, the response of the medium depends exclusively on the plasma frequency, $\nu_p = (n_e e^2)^{1/2}/(\pi m_e)^{1/2}$, and the cyclotron frequency, $\nu_B = eB/(2\pi m_e c)$. In the high frequency regime (i.e., $\nu_B/\nu \ll 1$, applicable to the submillimeter emission considered here given plausible magnetic field strengths), the rotation and conversion coefficients are (Melrose & McPhedran 2005; Swanson 1989)

$$\kappa^*_{V\,\mathrm{cold}} = (2\pi/c)(\nu_p^2 \nu_B/\nu^2)\cos\theta \quad (6)$$

$$\kappa^*_{Q\,\mathrm{cold}} = -(\pi/c)(\nu_p^2 \nu_B^2/\nu^3)\sin^2\theta\ , \quad (7)$$

where θ is the angle between the magnetic field vector and the line of sight. The ratio of these equations shows Faraday conversion (κ_V^*) to be a factor of ν_B/ν ($\sim 10^{-3}$ for our data) smaller than rotation, inconsistent with our observations. Equations for higher temperature plasmas are presented in section 5.6.

5.2. *Magnetic Field Changes*

Homan et al. (2009) list a series of scenarios in which CP can be produced in quasars. By incorporating line-of-sight changes in the magnetic field geometry, they offer possibilities not present in the homogenous-field radiative transfer equation (eq. 5). In a uniform field, Stokes Q needs to be converted into Stokes U before Stokes U can be converted into Stokes V. Changes in the field orientation along the line of sight break a fundamental assumption of eq. 5: the azimuthal angle (ϕ) between the field direction in the plane of the sky and the coordinate axis $\hat{\mathbf{e}}_1$ was defined to be zero. Changes in field direction will introduce a coupling of Q and V across the domains of magnetic orientation. The magnitude of the transfer coefficients also depends on the angle θ, introducing a small additional change in coupling. These field orientation changes, whether stochastic (Ruszkowski & Begelman 2002) or ordered (as in the helical fields of Beckert 2003) can also create significant CP. Both of these mechanisms are capable of producing the CP sign coherence observed in Sgr A*, although a small net bias to the field direction is important for the stochastic field.

5.3. *Self-Absorbed Faraday Conversion*

The wavelength-dependent size of Sgr A* indicates the importance of synchrotron self-absorption in the observed SED. The source size and brightness are determined by the variation of density, magnetic field, and electron energy distribution with radius/distance, although there are unbreakable degeneracies between these quantities even assuming power laws in radius without additional information or assumptions. A specific choice of jet structure can determine the structure in density/field/energy and match both size and flux (e.g., Markoff et al. 2007) and even variability timing (Falcke et al. 2009). Similarly, the assumption of, e.g., an equipartition magnetic field can specify the structure for an accretion flow while matching observations.

Polarimetric observations add new information regarding the source structure, potentially reducing the need

for unverifiable assumptions. The structure of Sgr A* is likely to be more complex than is captured by power-law models; this is particularly true at submillimeter wavelengths where the emission originates near the black hole. Complex magneto-hydrodynamic simulations and general relativistic radiative transfer (e.g., Huang et al. 2008; Mościbrodzka et al. 2009; Shcherbakov et al. 2010; Shcherbakov & Huang 2011) will more faithfully represent the true source properties near 345 GHz than few-parameter analytic models. Nevertheless, the smoothness of the average CP spectrum, the exclusive left-handedness of the polarization from 1.4 to 345 GHz, and the slow monotonic variation of the fractional polarization suggest that much insight can be gained from a simple conceptual model incorporating the ideas of self-absorbed synchrotron sources (e.g., de Bruyn 1976).

In the case of self-absorbed synchrotron sources, the specific intensity near frequency ν is dominated by the emission of electrons within a narrow energy range around $\gamma_{\rm rad}$. An electron with Lorentz factor $\gamma_{\rm rad}$ emits most of its radiative power at a frequency $\nu_c \sim \gamma_{\rm rad}^2 eB\sin\theta/(2\pi m_e c) = \gamma_{\rm rad}^2 \nu_{B\perp}$. The brightness temperature associated with the emitting electrons is related to this effective Lorentz factor by (e.g., Pacholczyk 1970; Rybicki & Lightman 1979) $k_B T_b = \alpha(p)\gamma_{\rm rad} m_e c^2$, where $\alpha(p)$ is a coefficient of order unity. The brightness temperature can be obtained directly from observations: $T_b = 1.22\times10^{12} S_\nu \nu^{-2}\theta_s^{-2}(\nu)$ K; where S_ν is the observed flux density in Jy, θ_s is the source angular radius in milliarcseconds, and ν is in GHz. Assuming power-law dependencies of the form $S_\nu \propto \nu^{-m}$ and $\theta_s(\nu)\propto\nu^{-n}$, we obtain $\gamma_{\rm rad}\propto\nu^{-m-2+2n}$ (see, for example, Loeb & Waxman 2007).

5.4. *Self-Absorbed, Stratified Sources*

In what follows, our main approximation is to assume that at each frequency, the synchrotron-emitting electrons, with energies $\gamma_{\rm rad}$, are also responsible for Faraday conversion. We also assume that Faraday rotation and conversion can be considered to act in an alternating manner rather than attempting to treat the full, complicated PRT equation. The radiative transfer near the $\tau=1$ surface is particularly complicated because all matrix elements can be important. By assuming sequential effects, we can operator-split the differential equation. In this case, and for short propagation distances, the production of Stokes V is simply an angle of rotation in the Poincaré sphere corresponding to the cumulative phase shift between the polarization modes of the plasma near radius r_0 (Kennett & Melrose 1998). This can be calculated as an integral of κ_Q^*,

$$\Delta\psi(r_0,\nu) = \int_{r_0}^{\infty} \frac{\pi}{c}\frac{\nu_p^2\nu_B^2}{\nu^3}\sin^2\theta\ \Theta_{\rm FC}\ dr \quad , \tag{8}$$

where we have corrected the cold-plasma Faraday conversion rate (eq. 7) by a factor $\Theta_{\rm FC}$ (see Section 5.6 below) that takes into account the effect of a power-law distribution of relativistic electrons on Faraday conversion.

Following the treatment of Faraday conversion presented by Kennett & Melrose (1998), we take the finite-temperature correction to be proportional to the local mean Lorentz factor of the electron distribution, and we further approximate this with our value of $\gamma_{\rm rad}$ (in the same approximation $\Theta_{\rm FR}\sim\log\langle\gamma\rangle/\langle\gamma\rangle$; e.g., Sazonov 1969; Quataert & Gruzinov 2000),

$$\Theta_{\rm FC}(\nu,T_e,\theta,B)\sim\langle\gamma(r)\rangle\sim\gamma_{\rm rad} \quad . \tag{9}$$

Assuming conversion in a narrow range in r, we write

$$\begin{aligned}\Delta\psi(r_0,\nu) &\propto \int_{r_0}^{\infty} n_e(r)B(r)^2\sin^2\theta\ \gamma_{\rm rad}(r)\nu^{-3}dr \\ &\sim n_e(r_0)B(r_0)^2\ \gamma_{\rm rad}(r_0)\nu^{-3}r_0 \quad .\end{aligned} \tag{10}$$

We can obtain $\Delta\psi$ as a function of frequency by using the fact that for each observed frequency ν_0, there is a corresponding radius r_0. If we assume, as well, that the electron density and magnetic field have radial profiles of power-law form, $n_e\sim r^{-\beta}$ and $B\sim r^{-\alpha}$, the Faraday conversion phase shift is

$$\Delta\psi(r_0,\nu_0)\sim r_0^{-\beta-2\alpha+1}\nu_0^{-m+2n-5}\sim\nu^{\beta n+2\alpha n-m+n-5} \quad . \tag{11}$$

Power-law relations of the form $S_\nu\propto\nu^{-m}$—for the flux density—and $\theta_s(\nu)\propto\nu^{-n}$—for the source angular size—are a natural consequence of stratified synchrotron sources (de Bruyn 1976). In this simple model, the size-frequency relation is obtained as follows. First, we take the synchrotron optical depth associated with a narrow shell of radius r (Rybicki & Lightman 1979): $\tau_\nu(r)=\alpha_\nu\Delta r\sim n_e(r)B^{(p+2)/2}(r)\nu^{-(p+4)/2}r\sim r^{-\beta-\alpha(p+2)/2+1}\nu^{-(p+4)/2}$, where p is the electron power-law index. Hence, for a given frequency ν_0, the $\tau=1$-surface occurs at $r_0^{-\beta-\alpha(p+2)/2+1}\nu_0^{-(p+4)/2}\sim1$ or $r_0\sim\nu_0^{-(p+2)/(2\beta+\alpha(p+2)-2)}$. Similarly, the flux density can be shown to be (see de Bruyn 1976, for details) $S_\nu\sim\nu^{(13-5\beta-3\alpha-2\alpha p+2p)/(2-2\beta-2\alpha-\alpha p)}$. The resulting spectral indices are

$$\begin{aligned} n &= \frac{p+4}{2\beta+\alpha(p+2)-2} \quad \text{and} \\ m &= -\frac{13-5\beta-3\alpha-2\alpha p+2p}{2-2\beta-2\alpha-\alpha p} \quad . \end{aligned} \tag{12}$$

Therefore, α and β can be solved for as functions of m and n:

$$\begin{aligned} \beta &= \frac{-3-2m+5n-2p-mp+2np}{n} \quad \text{and} \\ \alpha &= \frac{5+2m-4n}{n} \quad , \end{aligned} \tag{13}$$

which gives (dropping the subscript in ν_0 for clarity)

$$\begin{aligned}\Delta\psi\sim\nu^l, \quad \text{with}\ \ l &= (2n-m-2)(p-1) \\ &= \frac{(p-1)(-\alpha+\beta-1)}{\alpha(p+2)+2(\beta-1)} \quad .\end{aligned} \tag{14}$$

The indices α and β are very sensitive to n, which is close to 1. Falcke et al. (2009) report a value of $n=1.3\pm0.1$, obtained from observations between 22 GHz and 230 GHz, after correcting for interstellar scattering. These results are very sensitive to the scattering model. Another approach, used by Shen (2006), is to minimize the dependence on the scattering law by relying on the shortest wavelength data. For measurements at 43 and 86 GHz, their result is $n=1.09\pm0.3$. An even shallower slope can be obtained using the results from Doeleman

et al. (2008). From the VLBI visibilities, the angular size of the source, assuming a circular gaussian profile, is 37 μas, which is smaller than the last photon orbit for a Schwarzschild black hole (~ 52 μas). If the source geometry is assumed to be an annulus (Doeleman et al. 2008), the mean diameter is 58 μas. Using this angular diameter at 230 GHz gives a value of $n \sim 0.8$. In particular, for this value of n, with $m = -0.43$ (An et al. 2005), and assuming an electron power-law index of 2.4, we obtain $\alpha \sim 1.2$ and $\beta \sim 1.4$. These values are close to those corresponding to spherical accretion and equipartition of energy ($\beta = 3/2$ and $\alpha = (\beta + 1)/2 = 5/4$). Most importantly, these indices imply $l \sim 0.1$, i.e., the CP production rate is almost independent of frequency, which is consistent with observations (ranging from 0.5% to 1.5%) across a range in frequency of almost two orders of magnitude. The main point here is that a mild increase of CP with frequency is possible. Although this is contrary to the decreasing efficiency of Faraday conversion with frequency that is expected for a uniform medium, it is a natural consequence of stratified emission.

5.5. *Magnetic Field Structure and Polarization Stability*

The amount of CP generated from LP is proportional to this phase shift, i.e., $m_c \sim m_l \, \Delta\psi$ for small $\Delta\psi$. The weak dependence of $\Delta\psi$ on frequency implies that CP production in different layers of the source behaves similarly regardless of location respect to the SBMH. The value of $\Delta\psi$ should remain small to avoid conversion of CP back to LP at high frequencies. Starting with the $\sim 10\%$ (e.g., Pacholczyk 1970) intrinsic polarization fraction of the optically thick synchrotron, achieving CP fractions of 0.1% to 1% requires $\Delta\psi \sim 0.01$–0.1. Such small values are far from reversing the sign of CP, consistent with the fixed sign of CP at all frequencies, as long as the orientation of the orientation magnetic field does not fluctuate randomly. A variable orientation of the magnetic field with radius—i.e., field reversals—is inconsistent with the apparent self-similarity of the CP spectrum. If this self-similarity persists for more than two orders of magnitude in frequency (1 to 345 GHz), the orientation of the magnetic field must be highly coherent over spatial scales spanning nearly two orders of magnitude (since $n \approx 1$), roughly between $1R_S$ and $100R_S$.

In plane-of-the-sky coordinates aligned with $\mathbf{B}_{\rm sky}$ (total field equals plane-of-the-sky field $\mathbf{B}_{\rm sky}$ plus line-of-sight field $\mathbf{B}_{\rm los}$), eq. 5 shows that for intrinsic synchrotron emission only in I and Q, Faraday conversion proceeds as $Q \rightarrow U \rightarrow V$, i.e., conversion is driven by Faraday rotation within a narrow synchrotron shell (Beckert 2003). The sign of U generated by this mechanism depends on the sign of the Faraday rotation coefficient κ_V^* (eq. 6), which can change depending on the angle the magnetic field makes with respect to the line of sight θ. On the other hand, the sign of the Faraday conversion coefficient κ_Q^* (eq. 7) does not change with θ. This implies that the sign of Stokes V generated by conversion is exclusively determined by the sign of Stokes U generated from Q by local Faraday rotation, and is ultimately dependent on the local value of $\cos\theta$. Therefore, a constant sign in Stokes V needs a constant orientation of $\mathbf{B}_{\rm los}$. This requirement is already hinted at by the observed RM properties (Marrone et al. 2006a, 2007). On the other hand, the orientation of $\mathbf{B}_{\rm sky}$ is free to change in time without affecting the value of V. This is a consequence of the sequence $Q \rightarrow U \rightarrow V$ given by eq. 5, where the first step is performed by Faraday rotation depending only on $\mathbf{B}_{\rm los}$ and the fact that Stokes V does not change with coordinate transformations in the plane of the sky. Changes of the orientation of $\mathbf{B}_{\rm sky}$ in time will only change the observer's definition of Stokes Q and U. Indeed, this is likely to be the explanation for the observed wandering values of Q and U (Marrone et al. 2006b), while Stokes V appears to be stable.

5.5.1. *Relation to Observed Faraday Rotation Rates*

A key assumption in the self-absorbed approximation above is that synchrotron emission, Faraday conversion, and Faraday rotation (which drives conversion) all take place within the same narrow shell of plasma. Previous work (e.g., Marrone et al. 2007) has assumed that Faraday rotation primarily occurs far from the emission region at a given frequency. This "Faraday screen" approximation may still operate in regions of the accretion envelope where the material is too optically thin to contribute any emission or absorption to the incoming radiation while still being dense and magnetized enough to produce Faraday rotation. For such cases, Marrone et al. (2006a) calculate the cumulative Faraday rotation acting upon polarized radiation emitted at radius r_0 (analogous to eq. 8) as

$$\Delta\chi(r_0, \nu) = \int_{r_0}^{\infty} \frac{2\pi}{c} \frac{\nu_p^2 \nu_B}{\nu^2} \cos\theta \; \Theta_{\rm FR} \; dr \quad , \tag{15}$$

(except for the $\Theta_{\rm FR}$ term, which is taken to be 1). The total emission (Stokes I, V, and total LP) is assumed to come from a region interior to r_0 and to be essentially unaffected as it emerges from the source, except for the Faraday rotation of the electric vector position angle (EVPA).

To be consistent with our self-absorbed Faraday conversion approach, Faraday rotation should act both internally (at $\tau \sim 1$, where it drives conversion) as well as externally (at $\tau \ll 1$, where the Faraday screen approximation is valid). To satisfy this requirement, the Faraday rotation scale lengths should extend far beyond the thickness of the emission/conversion shell. To confirm this, we define the differential Faraday rotation and conversion depths (differential forms of eqs. 8 and 15) as

$$\frac{d\tau_{\rm FR}}{dr} \propto r^{-(\beta+\alpha)} \Theta_{\rm FR}(r) \nu^{-2} \approx r^{-(\beta+\alpha)} \frac{\ln \gamma_{\rm rad}(r)}{\gamma_{\rm rad}(r)} r_0^{2n} \tag{16}$$

and

$$\frac{d\tau_{\rm FC}}{dr} \propto r^{-(\beta+2\alpha)} \Theta_{\rm FC}(r) \nu^{-3}, \approx r^{-(\beta+2\alpha)} \gamma_{\rm rad}(r) r_0^{3n} \quad , \tag{17}$$

respectively, where $\gamma_{\rm rad} \propto r^{-\delta}$ (Section 5.3) is also a power law of r, with δ small. It can be readily seen that $d\tau_{\rm FC}/dr$ is significantly steeper in radius than $d\tau_{\rm FR}/dr$. For comparison, the synchrotron optical depth can be written in differential form as $d\tau/dr \sim r^{-\beta-\alpha(p+2)/2} \nu^{-(p+4)/2}$ (see Section 5.3). For values of p between 2 and 3, $d\tau/dr$ can be as steep as or steeper than $d\tau_{\rm FC}/dr$, and thus also steeper than $d\tau_{\rm FR}/dr$, confirming

that significant Faraday rotation takes place outside of the $\tau = 1$ surface (see Jones & Odell 1977). This means that Faraday rotation is still at work when Faraday conversion has stopped being effective. In other words, the source has only a limited spatial range to produce Stokes V—driven by the sequence $Q \rightarrow U \rightarrow V$—before the conversion rate decreases to negligible values. Therefore, while Faraday conversion is roughly local to the shell of radius r_0, Faraday rotation is not.

A consequence of having significant Faraday rotation within and immediately outside the photosphere is a frequency-dependent rotation measure. The highest frequencies probe deeper layers in the stratified source and therefore integrate Faraday rotation contributions from the shells that define lower-frequency photospheres. There are, as of yet, few observational constraints on this possibility. The RM has been determined through the measurement of a change in χ across a narrow range in frequency (Marrone et al. 2007), and less securely through the comparison of position angles averaged over several observations at more widely separated frequencies (Macquart et al. 2006). A demonstration of the frequency dependence of the RM could be obtained through position angle measurements at multiple pairs of closely spaced frequencies, which should be possible very soon with improved millimeter interferometers and ALMA.

Although the Faraday screen approximation is reasonable for a stratified synchrotron source, it can be difficult to obtain an accurate RM observationally, due to the source's layered geometry. Assuming the cold, optically thin Faraday rotation relation $\chi(\nu) = \chi_0 + c^2/\nu^2 \mathrm{RM}$ (e.g., Marrone et al. 2006a, eq. 1), RM is observationally obtained by computing the quantity $d\chi/d\lambda^2 = d\chi/d(c/\nu^2) \approx \Delta\chi/\Delta(c^2/\nu^2)$, using two neighboring frequencies and their respective observed EVPAs. The implied assumption, in addition to the validity of the screen, is that the emission at the two observed frequencies is originated in the same region and with the same initial EVPA χ_0. However, in the layered scenario, if these two frequencies correspond to two shells that do not overlap spatially, they will produce emission that will travel through two different Faraday screens. In that case, RM would be a function of the two frequencies observed and not a constant value. Thus far, observations suggest that this is not the case and that RM is indeed a constant, even when χ_0 varies in time (Marrone et al. 2007). Simultaneous observations at more than two frequencies will help resolve the question of whether Faraday rotation in Sgr A* is proportional to ν^{-2} or not.

One unaddressed problem in the discussion above is that there apparently is not enough observed LP at low frequencies, (e.g., 4 and 8 GHz, where CP dominates) to generate the observed Stokes V via the Faraday conversion process. However, synchrotron flux density is highly polarized for ordered magnetic fields, even in the optically thick limit (Pacholczyk 1970). Therefore, it is highly likely that the observed LP suffers severe beam smoothing at these frequencies, at a point beyond the conversion region, if the Faraday-rotation region shows fluctuations (e.g., stochastic or turbulent in nature) at spatial scales smaller than the source size. For the sake of argument, consider partially polarized radiation with constant polarization angle χ_0 entering a piecewise uniform Faraday screen. Radiation will exit the screen with rms fluctuations in EVPA equal to $\sigma_\chi \sim \sigma_{\rm RM}(c/\nu)^2$, where $\sigma_{\rm RM}$ contains the fluctuations in n_e, B, and θ. If the fluctuations in the outcoming $\Delta\chi$ are Gaussian, the observed LP will be $\langle m_l \rangle = m_{l,0}\, e^{-2\sigma_\chi^2}$, where $m_{l,0}$ is the original LP fraction entering the screen. This occurs because, while Q and U are additive quantities, total LP is not, resulting in observed values of m_l that are severely sensitive to EVPA changes in the plane of the sky.

5.6. *The Faraday Conversion at Finite Temperatures*

In an accretion flow, many of the physical quantities relevant for synchrotron emission are expected to increase inwardly. This is true for the electron density n_e and the temperature T. In particular, the temperature of the plasma near the event horizon can achieve mildly to highly relativistic temperatures. It is evident then that the cold plasma approximation should not apply in the interior regions where Faraday conversion could operate. A more general expression for the Faraday transport coeffcients (eqs. 6 and 7) is

$$\begin{aligned}\kappa_V^* &= \frac{2\pi}{c}\frac{\nu_p^2\nu_B}{\nu^2}\cos\theta\,\Theta_{\rm FR}(\nu, T_e, \theta, B) \\ &= \kappa_{V\,\rm cold}^*\,\Theta_{\rm FR}(\nu, T_e, \theta, B)\end{aligned} \tag{18}$$

$$\begin{aligned}\kappa_Q^* &= -\frac{\pi}{c}\frac{\nu_p^2\nu_B^2}{\nu^3}\sin^2\theta\,\Theta_{\rm FC}(\nu, T_e, \theta, B) \\ &= \kappa_{Q\,\rm cold}^*\,\Theta_{\rm FC}(\nu, T_e, \theta, B)\quad ,\end{aligned} \tag{19}$$

where the functions $\Theta_{\rm FR}(\nu, T_e, \theta, B)$ and $\Theta_{\rm FC}(\nu, T_e, \theta, B)$ are finite-temperature corrections to the standard cold-plasma transport coefficients. By definition, $\Theta_{\rm FR,FC} \rightarrow 1$ when $T \rightarrow 0$ and $\nu \gg \nu_B$.

In a cold plasma, the electrons oscillate in response to electromagnetic waves but are effectively stationary otherwise. When the electron energy distribution is non-negligible, the interaction of electron motions and incident electromagnetic radiation is given by the Boltzmann equation in the presence of the Lorentz force: the Vlasov equation. The Vlasov equation describes the dielectric tensor of the plasma and thus its Faraday transport coefficients, which depend on the electron energy distribution (e.g., Melrose & McPhedran 2005).

One of the earliest approaches to this problem originated with Sazonov (1969). For a power-law distribution of electron energies, the ratio of the Faraday transport coefficients (see also Jones & Odell 1977) is

$$\begin{aligned}\left|\frac{\kappa_Q^*}{\kappa_V^*}\right|_{\rm pl} &= \left|\frac{\kappa_Q^*}{\kappa_V^*}\right|_{\rm cold}\frac{\Theta_{\rm FC}^{\rm pl}}{\Theta_{\rm FR}^{\rm pl}} = \left|\frac{\kappa_Q^*}{\kappa_V^*}\right|_{\rm cold} \\ &\times \frac{2(p+1)}{(p+2)(p-2)}\frac{\gamma_{\rm min}^3}{\ln\gamma_{\rm min}}\left[1 - \left(\gamma_{\rm min}^2\frac{\nu_{B\perp}}{\nu}\right)^{\frac{(p-2)}{2}}\right]\quad ,\end{aligned} \tag{20}$$

which is an increasing function of $\gamma_{\rm min}$ ($\gamma_{\rm min} > 1$ always) under the condition $\nu_B/\nu \ll 1$. Eq. 20 shows that even with $\left(\kappa_Q^*/\kappa_V^*\right)_{\rm cold} \ll 1$, for hot enough plasmas, the Faraday conversion coefficient κ_Q^* can become a significant fraction of κ_V^* or even exceed it in extreme cases.

For electrons in a relativistic thermal (Maxwell-Juttner) distribution, the plasma dielectric tensor is different. Melrose (1997) derived an ultrarelativistic approximation for the response tensor of a magnetized thermal plasma. Ballantyne et al. (2007) combined this result with that of a classical cold plasma to obtain an approximate continuous function of the polarization proper modes as a function of temperature. Shcherbakov (2008) extended these results, providing consistent analytic expressions valid for all temperatures. In this case, the ratio of the Faraday transport coefficients is

$$\left|\frac{\kappa_Q^*}{\kappa_V^*}\right|_{\rm therm} = \left|\frac{\kappa_Q^*}{\kappa_V^*}\right|_{\rm cold} \frac{\Theta_{\rm FC}^{\rm therm}}{\Theta_{\rm FR}^{\rm therm}} = \left|\frac{\kappa_Q^*}{\kappa_V^*}\right|_{\rm cold} \left[\frac{K_1\left(\frac{m_e c^2}{k_B T}\right)}{K_0\left(\frac{m_e c^2}{k_B T}\right)} + 6\frac{k_B T}{m_e c^2}\frac{K_2\left(\frac{m_e c^2}{k_B T}\right)}{K_0\left(\frac{m_e c^2}{k_B T}\right)}\right] \frac{g\left(T,\theta,\nu_B/\nu\right)}{f\left(T,\theta,\nu_B/\nu\right)} \quad , \tag{21}$$

where $K_n(x)$ is the modified Bessel function of the second kind. Eq. 21 smoothly reduces to the cold plasma limit when $T \to 0$, since the term in the square brackets becomes exactly 1 in this limit. At temperatures of 10^9K ($kT/m_e c^2 = 1/6$), the term in the square brackets takes a value of ~ 2.5, and at 2×10^{11}K ($kT/m_e c^2 = 34$), it reaches $\sim 1.3 \times 10^5$.

The factors f and g, above, introduced by Shcherbakov (2008), take a value of 1 for $\nu_B/\nu \to 0$ and provide the necessary corrections for higher-order terms in ν_B/ν. They can lead to significant modifications to the ratio of the Faraday transport coefficients in the moderately relativisitic regime. For example, for intense magnetic fields, the cyclotron frequency can be written $\nu_B = 0.35\,{\rm GHz}\,(B/20{\rm G})$, and thus the ratio ν_B/ν takes values of $\sim 10^{-3}$ at submillimeter wavelengths. Following Shcherbakov (2008), at $\nu_B/\nu = 10^{-3}$ and $T = 2 \times 10^{11}$ K with $\theta = \pi/4$, the correction factors become $g \sim 0.93$ and $f \sim -0.003$. The multipliers of the cold Faraday transport coefficients in eq. 21 can strongly change the expected behavior even at moderate temperatures. This clearly demonstrates the importance of including these factors in numerical simulations of Sgr A* in order to properly handle the PRT problem.

6. CONCLUSIONS

We have reported the first detection of circularly polarized radiation toward Sagittarius A* at submillimeter wavelengths. The detected CP fractions are at levels of $1.2 \pm 0.3\%$ and $1.6 \pm 0.3\%$ for 230 GHz and 345 GHz, respectively, and are confirmed by observations at different epochs. We have tested the significance of this detection by analyzing the gain calibration, spectral variability and time variability, and by observing other sources. CP is not found in any other source, with the most sensitive limits confining uncalibrated instrumental CP to less than 0.2%.

Our measurements of CP, combined with previously reported measurements at lower frequencies, indicate that the polarization fraction rises with frequency. The sign (handedness) of the CP signal is the same for all detections at all frequencies over the period 1981 to 2007, as was found in low-frequency measurements alone (e.g., Bower et al. 2002). The average CP fraction as a function of frequency is remarkably well characterized by a power law with $\nu^{0.35\pm0.03}$. However, there have been no detections of CP between 15 and 230 GHz, so the CP spectrum may not be monotonic.

The general trend of slowly increasing CP with frequency is consistent with self-absorbed Faraday conversion. We discuss a simple set of power-law scalings of B and n_e that allow Faraday conversion to operate with only weak frequency dependence, imposing no CP sign reversals as long as the magnetic field itself does not reverse over the range of radii providing centimeter to submillimeter emission. In contrast, more sophisticated models in the literature (Huang et al. 2008, 2009a) show frequent reversals in submillimeter CP and therefore are not consistent with the results presented here.

If the CP originates from self-absorbed Faraday conversion, the corresponding Faraday rotation depth could vary with frequency, which would be contrary to the assumption of a cold Faraday screen (Macquart et al. 2006; Marrone et al. 2007). Polarization observations in the near future will test the frequency variation of the RM, and there already exists a claim of an RM change between 22 and 230 GHz (Yusef-Zadeh et al. 2007). In general, the PRT in a self-absorbed synchrotron source should couple the variations in LP and CP, so sensitive observations of variability in the polarization of this source will be crucial to understanding the structure of the emission region and the source of CP. As with variations in the RM (Sharma et al. 2007; Pang et al. 2011), variations in CP will occur on a timescale set by the structure of the accretion flow and can therefore differentiate between models.

Acknowledgments. We thank Avery Broderick, Siming Liu, and Roman Shcherbakov for helpful comments and discussions. Support for DPM was provided by NASA through Hubble Fellowship grant HST-HF-51259.01 awarded by the Space Telescope Science Institute, which is operated by the Association of Universities for Research in Astronomy Inc. for NASA, under contract NAS 5-26555.

Facilities: SMA (Polarimeter)

REFERENCES

Aitken, D. K., Greaves, J., Chrysostomou, A., et al. 2000, ApJ, 534, L173
An, T., Goss, W. M., Zhao, J.-H., et al. 2005, ApJ, 634, L49
Ballantyne, D. R., Özel, F., & Psaltis, D. 2007, ApJ, 663, L17
Beckert, T. 2003, Ap&SS, 288, 123
Beckert, T. & Falcke, H. 2002, A&A, 388, 1106
Blandford, R. D. & Begelman, M. C. 1999, MNRAS, 303, L1
Blundell, R. 2004, in Proc. 15th International Symposium on Space Terahertz Technology, ed. G. Narayanan (Northampton, MA: Univ. of Massachusetts), 3
Bower, G. C., Backer, D. C., Zhao, J., Goss, M., & Falcke, H. 1999a, ApJ, 521, 582
Bower, G. C., Falcke, H., & Backer, D. C. 1999b, ApJ, 523, L29
Bower, G. C., Falcke, H., Sault, R. J., & Backer, D. C. 2002, ApJ, 571, 843
Bower, G. C., Falcke, H., Wright, M. C., & Backer, D. C. 2005, ApJ, 618, L29
Bower, G. C., Goss, W. M., Falcke, H., Backer, D. C., & Lithwick, Y. 2006, ApJ, 648, L127

Bower, G. C., Wright, M. C. H., Backer, D. C., & Falcke, H. 1999c, ApJ, 527, 851
Bower, G. C., Wright, M. C. H., Falcke, H., & Backer, D. C. 2001, ApJ, 555, L103
—. 2003, ApJ, 588, 331
Broderick, A. E., Fish, V. L., Doeleman, S. S., & Loeb, A. 2011, ApJ, 738, 38
de Bruyn, A. G. 1976, A&A, 52, 439
Dexter, J., Agol, E., & Fragile, P. C. 2009, ApJ, 703, L142
Doeleman, S. S., Weintroub, J., Rogers, A. E. E., et al. 2008, Nature, 455, 78
Falcke, H., Mannheim, K., & Biermann, P. L. 1993, A&A, 278, L1
Falcke, H. & Markoff, S. 2000, A&A, 362, 113
Falcke, H., Markoff, S., & Bower, G. C. 2009, A&A, 496, 77
Fish, V. L., Doeleman, S. S., Beaudoin, C., et al. 2011, ApJ, 727, L36+
Ghez, A. M., Salim, S., Weinberg, N. N., et al. 2008, ApJ, 689, 1044
Gillessen, S., Eisenhauer, F., Trippe, S., et al. 2009, ApJ, 692, 1075
Ho, P. T. P., Moran, J. M., & Lo, K. Y. 2004, ApJ, 616, L1
Homan, D. C., Lister, M. L., Aller, H. D., Aller, M. F., & Wardle, J. F. C. 2009, ApJ, 696, 328
Homan, D. C. & Wardle, J. F. C. 1999, AJ, 118, 1942
Huang, L., Liu, S., Shen, Z.-Q., et al. 2008, ApJ, 676, L119
Huang, L., Liu, S., Shen, Z.-Q., et al. 2009a, ApJ, 703, 557
Huang, L., Takahashi, R., & Shen, Z. 2009b, ApJ, 706, 960
Jones, T. W. & Odell, S. L. 1977, ApJ, 214, 522
Kennett, M. & Melrose, D. 1998, PASA, 15, 211
Kunneriath, D. et al. 2010, A&A, 517, A46+
Landau, L. D. & Lifshitz, E. M. e. 1975, The Classical Theory of Fields (Oxford: Pergamon Press)
Loeb, A. & Waxman, E. 2007, Journal of Cosmology and Astro-Particle Physics, 3, 11
Macquart, J.-P., Bower, G. C., Wright, M. C. H., Backer, D. C., & Falcke, H. 2006, ApJ, 646, L111
Mahadevan, R., Narayan, R., & Yi, I. 1996, ApJ, 465, 327
Maitra, D., Markoff, S., & Falcke, H. 2009, A&A, 508, L13
Markoff, S., Bower, G. C., & Falcke, H. 2007, MNRAS, 379, 1519
Markoff, S., Falcke, H., Yuan, F., & Biermann, P. L. 2001, A&A, 379, L13
Marrone, D. P. 2006, PhD thesis, Harvard University
Marrone, D. P., Moran, J. M., Zhao, J.-H., & Rao, R. 2006a, ApJ, 640, 308
—. 2006b, Journal of Physics Conference Series, 54, 354
—. 2007, ApJ, 654, L57
Marrone, D. P. & Rao, R. 2008, in Society of Photo-Optical Instrumentation Engineers (SPIE) Conference Series, Vol. 7020, 60
Marrone, D. P., Baganoff, F. K., Morris, M. R., et al. 2008, ApJ, 682, 373
Melia, F., Liu, S., & Coker, R. 2001, ApJ, 553, 146
Melrose, D. B. 1997, Journal of Plasma Physics, 58, 735
Melrose, D. B. & McPhedran, R. C. 2005, Electromagnetic Processes in Dispersive Media (Cambridge, UK: Cambridge Univ. Press)
Mościbrodzka, M., Gammie, C. F., Dolence, J. C., Shiokawa, H., & Leung, P. K. 2009, ApJ, 706, 497
Narayan, R., Mahadevan, R., Grindlay, J. E., Popham, R. G., & Gammie, C. 1998, ApJ, 492, 554
Narayan, R. & Yi, I. 1994, ApJ, 428, L13
Pacholczyk, A. G. 1970, Radio Astrophysics: Nonthermal Processes in Galactic and Extragalactic Sources (San Francisco: Freeman)
Pang, B., Pen, U.-L., Matzner, C. D., Green, S. R., & Liebendörfer, M. 2011, MNRAS, 415, 1228
Quataert, E. & Gruzinov, A. 2000, ApJ, 539, 809
Ruszkowski, M. & Begelman, M. C. 2002, ApJ, 573, 485
Rybicki, G. B. & Lightman, A. P. 1979, Radiative Processes in Astrophysics (New York: Wiley-Interscience)
Sault, R. J. & Macquart, J.-P. 1999, ApJ, 526, L85
Sault, R. J., Teuben, P. J., & Wright, M. C. H. 1995, in Astronomical Data Analysis Software and Systems IV (ASP Conf. Ser. 77), ed. R. A. Shaw, H. E. Payne, & J. J. E. Hayes (San Francisco, CA: ASP), 433
Sazonov, V. N. 1969, Soviet Astronomy, 13, 396
Sharma, P., Quataert, E., & Stone, J. M. 2007, ApJ, 671, 1696
Shcherbakov, R. V. 2008, ApJ, 688, 695
Shcherbakov, R. V. & Huang, L. 2011, MNRAS, 410, 1052
Shcherbakov, R. V., Penna, R. F., & McKinney, J. C. 2010, (submitted to ApJ) arXiv:1007.4832,
Shen, Z.-Q. 2006, Journal of Physics Conference Series, 54, 377
Shen, Z.-Q., Lo, K. Y., Liang, M.-C., Ho, P. T. P., & Zhao, J.-H. 2005, Nature, 438, 62
Swanson, D. G. 1989, Plasma Waves (Boston: Academic Press)
Thompson, A. R., Moran, J. M., & Swenson, Jr., G. W. 2001, Interferometry and Synthesis in Radio Astronomy, 2nd ed. (New York: Wiley)
Tsuboi, M., Miyahara, H., Nomura, R., Kasuga, T., & Miyazaki, A. 2003, Astronomische Nachrichten Supplement, 324, 431
Wardle, J. F. C. & Homan, D. C. 2003, Ap&SS, 288, 143
Yuan, F., Markoff, S., & Falcke, H. 2002, A&A, 383, 854
Yuan, F., Quataert, E., & Narayan, R. 2003, ApJ, 598, 301
Yusef-Zadeh, F., Wardle, M., Cotton, W. D., Heinke, C. O., & Roberts, D. A. 2007, ApJ, 668, L47
Yusef-Zadeh, F., Wardle, M., Heinke, C., et al. 2008, ApJ, 682, 361